Subdiffusive motion of a polymer composed of subdiffusive monomers

Stephanie C. Weber
Department of Biochemistry and Howard Hughes Medical Institute, Stanford University, Stanford, California 94305, USA

Julie A. Theriot
Department of Biochemistry, Howard Hughes Medical Institute, Biophysics Program, and Department of Microbiology and Immunology, Stanford University, Stanford, California 94305, USA

Andrew J. Spakowitz
Biophysics Program and Department of Chemical Engineering, Stanford University, Stanford, California 94305, USA

(Received 6 December 2009; revised manuscript received 5 April 2010; published 19 July 2010)

We use Brownian dynamics simulations and analytical theory to investigate the physical principles underlying subdiffusive motion of a polymer. Specifically, we examine the consequences of confinement, self-interaction, viscoelasticity, and random waiting on monomer motion, as these physical phenomena may be relevant to the behavior of biological macromolecules *in vivo*. We find that neither confinement nor self-interaction alter the fundamental Rouse mode relaxations of a polymer. However, viscoelasticity, modeled by fractional Langevin motion, and random waiting, modeled with a continuous time random walk, lead to significant and distinct deviations from the classic polymer-dynamics model. Our results provide diagnostic tools—the monomer mean square displacement scaling and the velocity autocorrelation function—that can be applied to experimental data to determine the underlying mechanism for subdiffusive motion of a polymer.

DOI: 10.1103/PhysRevE.82.011913 PACS number(s): 87.17.−d, 87.15.Vv, 05.40.Jc, 83.60.Bc

I. INTRODUCTION

Much is known about the equilibrium and dynamic behavior of polymers through classical treatments of conventional polymeric materials and fluids [1]. It is desirable to leverage this wealth of knowledge to address a range of biomacromolecular phenomena. However, in many instances, new physical effects arise in biological systems that have not been previously addressed by polymer physics approaches. For example, the motion of a locus, or specific DNA segment, on a chromosome is potentially affected by confinement, cytoplasmic viscoelasticity, and binding interactions. This paper introduces these physical effects into the classical picture of polymer dynamics to determine their net impact on macromolecular behavior *in vivo*.

Chromosomal loci in prokaryotes [2,3] and eukaryotes [4,5] have been observed to move subdiffusively. This anomalous behavior is characterized by a non-linear relationship between mean square displacement (MSD) and time, such that $\langle[\vec{R}(t)-\vec{R}(0)]^2\rangle \sim t^{\alpha}$, where $0<\alpha<1$ [6]. Predictions from classical theories of polymer behavior do not agree with the observed scaling exponent α. This discrepancy raises the question of whether classic polymer-dynamics models can explain such scalings, or whether additional physical effects such as confinement, cytoplasmic viscoelasticity, and binding interactions must be applied to polymers to explain this behavior.

Subdiffusive motion of particles *in vitro* [7,8] and *in vivo* [9,10] has been explained using physical models incorporating fixed obstacles [11], environment viscoelasticity [12] and random waiting (binding) in the particle trajectory [13,14]. These three models generate similar scaling laws for long-time, ensemble-averaged particle behavior. Recent studies have identified other properties, such as ergodicity and first-passage-time statistics, that can be applied to experimental data to distinguish between these mechanisms [12,14–16].

Here, we apply such physical effects to the monomers in a polymer chain. In Sec. III, we perform Brownian dynamics simulations of a single polymer and find a robust Rouse-like monomer scaling, even under strong confinement and self-interaction. We proceed to address the additional role of environment viscoelasticity and random waiting in the context of the Rouse model for polymer dynamics. In Sec. IV, we study the motion of a single polymer chain in a viscoelastic environment, modeled using fractional Langevin motion (fLm). In Sec. V, we analyze the dynamic behavior of a polymer whose monomers experience random waiting, modeled as a continuous time random walk (CTRW). In each section, we follow our analytical derivation with a discussion of the physical intuition and scaling arguments that emerge from the theory. Our results provide diagnostic tools—the monomer MSD scaling and the velocity autocorrelation function—that can be applied to experimental data to determine the underlying mechanism for subdiffusive motion of a polymer as observed in a living cell.

II. POLYMER MODEL

The physical phenomena of interest occur at length and time scales where the polymer behavior is suitably captured by the Gaussian-chain model [1]. We define a polymer chain with length bN, where b is the Kuhn statistical segment length and N is the number of Kuhn segments within the chain. The chain configuration is defined by the coordinates of $M+1$ discrete effective monomers, where $\vec{R}_m$ is the mth monomer position ($m=0,1,2,\ldots,M$). Therefore, each inter-monomer segment has a discretization of $g=N/M$.

The configurational free energy of the polymer chain F_{conf} is defined according to the discrete Gaussian-chain model, such that

$$F_{conf} = \sum_{m=1}^{M} \frac{3k_BT}{2gb^2}(\vec{R}_m - \vec{R}_{m-1})^2, \tag{1}$$

where k_BT is thermal energy. This purely entropic free energy accounts for the entropic cost associated with the reduction in configurations available to each effective segment upon stretching the chain. In the absence of other free-energy contributions, this model results in a chain with mean square end-to-end distance $\langle(\vec{R}_M - \vec{R}_0)^2\rangle = b^2N$, which is notably independent of the discretization M. This property alludes to the fact that a Gaussian random walk is a continuous fractal, self-similar at all length scales, and invariant to discretization. This model is easily adapted to a circular polymer (as in plasmid DNA) by including a term in the configurational free energy joining monomer 0 with monomer M. We model both linear and circular polymers in this paper.

III. CONFINED POLYMER IN A NEWTONIAN FLUID

The chromosome of *Escherichia coli* is a single circular polymer with a contour length 1.6×10^6 nm. Each *E. coli* cell, with diameter ~ 1 μm, contains two to four copies of this circular chromosome. At this level of confinement, these polymers have considerable self-interaction that could potentially impact their dynamic behavior. However, the physical constraints on a confined polymer differ significantly from the assumptions made in existing polymer-dynamics theories. In this section, we adopt a simple approach to address the dynamics of the *E. coli* chromosome by considering a single polymer within a confinement that is much smaller than its unconfined radius of gyration.

The Rouse [17], Zimm [18] and reptation [19] models describe the motion of polymers in infinite solutions. These models do not consider how a polymer interacts with a boundary (i.e., the cell membrane). Furthermore, they assume that polymer chains are linear, which is particularly important for reptation, in which free ends must be able to explore space beyond the reptation tube for large-scale relaxations. Finally, de Gennes's reptation tube is defined by many polymer chains whose motions are uncorrelated with the entangled tracer chain. However, within a single polymer chain, the motion of one segment is correlated with all others, and the reptation tube will relax in concert with the tracer segment. Given these issues of confinement, topology and chain number, it is not clear whether the classic polymer-dynamics models are applicable to the motion of bacterial chromosomes *in vivo*. Thus, we use Brownian dynamics simulations to explore the scaling of a monomer on a single circular polymer under confinement.

Our simulations include five forces acting on each monomer in the chain. First, the configurational free energy F_{conf} results in an elastic restoring force

$$\vec{F}_m^{(E)} = \begin{cases} \frac{3k_BT}{gb^2}(\vec{R}_{m+1} - 2\vec{R}_m + \vec{R}_{m-1}), & m = 1, \ldots, M-1 \\ \frac{3k_BT}{gb^2}[(\vec{R}_1 - \vec{R}_0) - c(\vec{R}_0 - \vec{R}_M)], & m = 0 \\ \frac{3k_BT}{gb^2}[c(\vec{R}_0 - \vec{R}_M) - (\vec{R}_M - \vec{R}_{M-1})], & m = M, \end{cases} \tag{2}$$

where m is the monomer index and c is the ring closure factor, such that when $c=1$, the chain is circular and monomers $m=0$ and $m=M$ are connected. When $c=0$, the chain is linear with monomers $m=0$ and $m=M$ as end points. Second, the self-interaction force $\vec{F}_m^{(I)}$ accounts for the finite size of monomers and prevents chain crossing. This force is generally written as

$$\vec{F}_m^{(I)} = -\sum_{m' \neq m} \frac{\partial V_I(R_{m,m'})}{\partial R_{m,m'}} \vec{e}_{m,m'}, \tag{3}$$

where $R_{m,m'} = |\vec{R}_m - \vec{R}_{m'}|$ is the distance between monomers m and m', $\vec{e}_{m,m'} = (\vec{R}_m - \vec{R}_{m'})/|\vec{R}_m - \vec{R}_{m'}|$ is the unit vector between monomers m and m', and $V_I(R_{m,m'})$ is the two-body interaction potential. Since the nature of these interactions inside the cell is unknown, we test several different V_I, including the repulsive Gaussian potential, the Lennard-Jones potential, and the repulsive part of a Lennard-Jones potential. Third, the repulsive interaction between a monomer and the confining boundary is captured by the force

$$\vec{F}_m^{(C)} = \begin{cases} -A_{ex}(|\vec{R}_m| - r)^3 \frac{\vec{R}_m}{|\vec{R}_m|}, & |\vec{R}_m| > r \\ 0, & |\vec{R}_m| \leq r, \end{cases} \tag{4}$$

where A_{ex} is the strength of confinement and r is the radius of confinement. Fourth, a viscous drag force represents friction that opposes the motion of a monomer through the solvent. Hydrodynamic interactions are ignored as they are likely screened *in vivo* due to a high degree of macromolecular crowding [1]. This velocity-dependent force, characterized by the drag coefficient ξ, is given by $-g\xi\frac{d\vec{R}_m}{dt}$. Finally, a random Brownian force $\vec{F}_m^{(B)}$ arises from collisions between a monomer and solvent molecules. The variance of the magnitude of this force is given by the fluctuation-dissipation theorem

$$\langle \vec{F}_m^{(B)}(t) \vec{F}_{m'}^{(B)}(t') \rangle = 2k_BT\xi\delta_{m,m'}\delta(t-t')\mathbf{I}. \tag{5}$$

Inertial forces are ignored, since these are negligible in comparison to viscous drag. For each time step in the simulation, the Langevin equation of motion,

$$g\xi\frac{d\vec{R}_m(t)}{dt} = \vec{F}_m^{(E)}(t) + \vec{F}_m^{(I)}(t) + \vec{F}_m^{(C)}(t) + \vec{F}_m^{(B)}(t), \tag{6}$$

is solved using a Runge-Kutta algorithm.

Figure 1 shows the results of a series of simulations with a spherical confinement of decreasing radius r. In these simulations, we choose the model parameters to be $k_BT=1$,

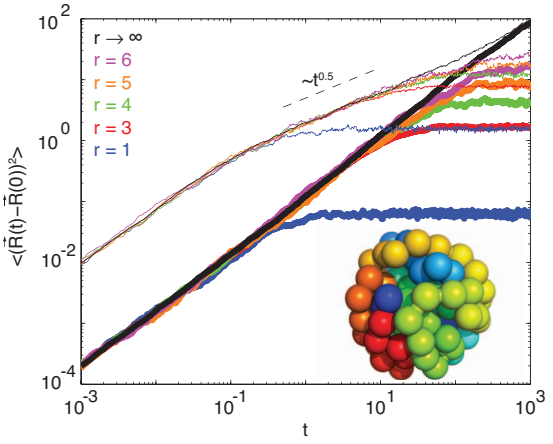

FIG. 1. (Color) Ensemble-averaged MSD of a monomer (thin curves) and the center-of-mass (thick curves) of a single circular polymer under spherical confinement. Data are from a series of simulations with Gaussian self-interaction and a decreasing radius of confinement, where: $r\to\infty$ (black), $r=6$ (pink), $r=5$ (orange), $r=4$ (green), $r=3$ (red), and $r=1$ (blue) (see text for parameter values). The inset shows a typical snapshot from the $r=3$ simulations.

$\xi=1$, $b=0.5477$, $g=1$, and $M=99$. This choice of dimensionless parameters is equivalent to rescaling the time by $10\xi(gb)^2/(3k_BT)$ and all lengths by $b\sqrt{10g/3}$, resulting in a strongly confined polymer chain for small confinement radius ($r<6$). When $r\to\infty$ (the free, unconfined case), the polymer behaves according to the Rouse model. The center-of-mass moves diffusively ($\alpha=1$) across all time scales, while the monomer moves diffusively at short and long times, but subdiffusively for intermediate times, with $\alpha=0.5$. As the radius of confinement decreases, the scaling exponents do not change until the polymer reaches the boundary and cannot diffuse further. Interestingly, even under extreme confinement, the subdiffusive scaling of a monomer is Rouse-like ($\alpha=0.5$) and not reptation-like ($\alpha=0.25$)

The intermediate-time scaling result found in Fig. 1 ($\alpha=0.5$) is robust across a broad range of simulation parameters. For example, the scaling of the monomer MSD is insensitive to all contour lengths tested ($4\le M\le 149$). It also does not depend on polymer topology; linear polymers exhibit the same α as circular polymers. Furthermore, the monomer MSD does not depend on the self-interaction potential. Our results for simulations with no self-interaction and for simulations incorporating three different interaction potentials (repulsive Gaussian, Lennard-Jones, and repulsive Lennard-Jones) give a robust scaling exponent $\alpha=0.51\pm0.02$ for intermediate times (Table I). Finally, we performed simulations with five polymers within a single confinement, and with this number of independent chains, we still observe Rouse-like scaling for the monomer MSD. This observation strongly suggests that the elastic Rouse modes dominate polymer behavior. Thus, it appears that the correlated motions of a single confined polymer annihilate the polymer's own reptation tube, leading to a Rouse-like intermediate-time scaling.

TABLE I. Intermediate-time scaling exponent α for simulations with no self-interaction, or a repulsive Gaussian, a Lennard-Jones or a repulsive Lennard-Jones interaction potential. Fits were made to the monomer MSD for at least one decade in time beginning at MSD=1 (i.e., beginning at the transition into the Rouse regime and ending before the monomer reaches the confining boundary). For confinement radius $r=1$, the monomer reaches the boundary before entering the Rouse regime and so does not exhibit a power law. Column 3 (repulsive Gaussian potential) corresponds to Fig. 1.

	Self-interaction potential			
Radius of confinement	None	Repulsive Gaussian	Lennard-Jones	Repulsive Lennard-Jones
$r\to\infty$	0.51	0.50	0.50	0.49
$r=6$	0.52	0.51	0.53	0.53
$r=5$	0.50	0.51	0.52	0.51
$r=4$	0.47	0.51	0.50	0.54
$r=3$	0.46	0.51	0.51	0.52
$r=1$	N/A	N/A	N/A	N/A

IV. POLYMER IN A VISCOELASTIC FLUID

In this section, we analyze the dynamic behavior of a single polymer within a viscoelastic medium. Our goal is to focus on the Rouse modes of such a polymer in the absence of self-interaction and confinement. With these approximations, we are able to find analytical results for experimentally observable metrics, including the monomer MSD and the velocity autocorrelation function. Our simulation results in the previous section suggest that the dominant scaling behavior for a confined polymer is associated with Rouse-like behavior, so our analyses in this section would adequately predict behavior under conditions of strong confinement and self-interaction.

A particle moving through a viscoelastic environment will undergo subdiffusive motion over a range of time scales due to elastic stresses within the medium. A further signature of viscoelasticity is the presence of time correlations in the particle's trajectory, also arising from elastic stresses. This viscoelastic behavior can be cast in terms of a fluid memory that propagates past deformation to the present response [1].

We consider a model for viscoelasticity that results in subdiffusive particle motion over all time scales. This model can be used to address physical phenomena over time scales where particle motion is experimentally observed to be subdiffusive. The particle is sufficiently small such that inertial effects are completely negligible. Mathematically, the motion of an isolated particle is governed by the fractional Langevin equation

$$\xi\int_0^t dt' K(t-t')\frac{d\vec{R}(t')}{dt}=\vec{F}^{(B)}(t), \tag{7}$$

where we adopt the memory kernel [12]

$$K(t-t')=\frac{(2-\alpha)(1-\alpha)}{|t-t'|^{\alpha}}, \tag{8}$$

and the Brownian force $\vec{F}^{(B)}(t)$ satisfies the fluctuation-dissipation theorem

$$\langle \vec{F}^{(B)}(t)\vec{F}^{(B)}(t')\rangle = \xi k_B T K(t-t')\mathbf{I}. \tag{9}$$

The power law in Eq. (8) persists over all time scales in the model, leading to particle subdiffusion over all time scales. Thus, the fractional Langevin motion (fLm) of this model results in a particle MSD

$$\langle [\vec{R}(t)-\vec{R}(0)]^2\rangle = \frac{3k_BT}{\xi}\frac{\sin(\alpha\pi)}{\pi\left(1-\frac{\alpha}{2}\right)(1-\alpha)\alpha}t^{\alpha}, \tag{10}$$

where $0<\alpha<1$ and smaller values of α correspond to more subdiffusive behavior. This behavior approaches $\langle[\vec{R}(t)-\vec{R}(0)]^2\rangle=(6k_BT/\xi)t$ as $\alpha\to 1$, corresponding to diffusion in a Newtonian fluid. Our definition of fLm is identical to previous treatments [12,20] with some minor alterations in the definition of parameters. Specifically, the Hurst parameter $H=1-\frac{\alpha}{2}$ typically appears in the definition of fractional Langevin motion; our preference is to define our model by α since this is the physical observable involved in all subsequent discussions.

We now consider a large linear polymer chain that is immersed in a medium that itself is viscoelastic. Our goal is to derive the behavior for an isolated ideal chain (i.e., no self-interaction) in the absence of long-range hydrodynamic interactions. In other words, our theoretical treatment introduces the fLm memory kernel into the classical Rouse model of polymer dynamics. The model for viscoelasticity defined above results in a governing equation of motion for the mth monomer in the chain

$$g\xi\int_0^t dt' K(t-t')\frac{d\vec{R}_m(t')}{dt} = \vec{F}_m^{(E)}(t)+\vec{F}_m^{(B)}(t), \tag{11}$$

where $\vec{F}_m^{(E)}(t)$ is given by Eq. (2), with $c=0$ to designate a linear chain with monomers $m=0$ and $m=M$ as end points. Our simulations in Sec. III show similar values of α at intermediate time scales for circular and linear chains, so we proceed with a linear chain topology in all following sections. Assuming N is large, we can pass the monomer index $m=0,1,\ldots,M$ to the continuous variable $n\in[0,N]$, resulting in the chain configuration defined by the space curve $\vec{r}(n,t)$. With this, we arrive at the governing differential equation

$$\xi\int_0^t dt' K(t-t')\frac{\partial\vec{r}(n,t')}{dt} = \frac{3k_BT}{b^2}\frac{\partial^2\vec{r}(n,t)}{\partial n^2}+\vec{f}^{(B)}(n,t), \tag{12}$$

where the Brownian force $\vec{f}^{(B)}(n,t)$ satisfies the fluctuation-dissipation theorem

$$\langle \vec{f}^{(B)}(n,t)\vec{f}^{(B)}(n',t')\rangle = \xi k_B T K(t-t')\delta(n-n')\mathbf{I}. \tag{13}$$

Since the chain ends are free and effectively unstressed, the boundary conditions on the polymer ends are $\partial_n\vec{r}(n=0,t)=\vec{0}$ and $\partial_n\vec{r}(n=N,t)=\vec{0}$.

As in the Rouse model [1], it is convenient to define a set of normal coordinates that effectively decouple the interactions implicit within the equation of motion [Eq. (12)]. We define the normal modes

$$\phi_p(n) = \begin{cases}\sqrt{2}\cos\left(\frac{p\pi n}{N}\right), & p=1,2,\ldots\\ 1, & p=0.\end{cases} \tag{14}$$

These modes represent a complete basis set that satisfy the boundary conditions for $\vec{r}(n,t)$; orthogonality is demonstrated by

$$\int_0^N dn\,\phi_p(n)\phi_{p'}(n) = N\delta_{p,p'}. \tag{15}$$

The amplitude of the pth mode $\vec{X}_p(t)$ is given by

$$\vec{X}_p(t) = \frac{1}{N}\int_0^N dn\vec{r}(n,t)\phi_p(n), \tag{16}$$

and the inversion back to chain coordinates is written as

$$\vec{r}(n,t) = \sum_{p=0}^{\infty}\vec{X}_p(t)\phi_p(n). \tag{17}$$

The equation of motion of the pth normal mode is written as

$$N\xi\int_0^t dt' K(t-t')\frac{d\vec{X}_p(t')}{dt} = -k_p\vec{X}_p(t)+\vec{F}_p^{(B)}(t), \tag{18}$$

where $k_p=[3\pi^2k_BT/(Nb^2)]p^2$, and the Brownian force on the pth mode $\vec{F}_p$ satisfies

$$\langle \vec{F}_p^{(B)}(t)\vec{F}_{p'}^{(B)}(t')\rangle = N\xi k_B T K(t-t')\delta_{p,p'}\mathbf{I}. \tag{19}$$

The resulting equation of motion [Eq. (18)] demonstrates the decoupling of the normal coordinates such that all normal coordinates are dynamically independent. Furthermore, the force on the pth mode $-k_p\vec{X}_p(t)$ corresponds to that of a harmonic spring with spring constant k_p. At equilibrium, the normal-mode amplitude satisfies the equipartition theorem $\langle\vec{X}_p(t)\vec{X}_{p'}(t)\rangle=\frac{k_BT}{k_p}\delta_{p,p'}\mathbf{I}$.

The chain dynamics are analyzed by defining the correlation function $C_p(t)=\langle\vec{X}_p(t)\cdot\vec{X}_p(0)\rangle$, which is governed by the differential equation

$$N\xi\int_0^t dt' K(t-t')\frac{dC_p(t')}{dt} = -k_pC_p(t) \tag{20}$$

with initial condition $C_p(t=0)=3k_BT/k_p$ for $p\geq 1$. Performing a Laplace transform of Eq. (20) from t to s, rearranging, and inverting, we arrive at the solution

$$C_p(t) = \frac{3k_BT}{k_p}E_{\alpha,1}\left[-\frac{k_p}{N\xi\Gamma(3-\alpha)}t^{\alpha}\right], \tag{21}$$

where $E_{\alpha,\beta}(x)$ is the generalized Mittag-Leffler function

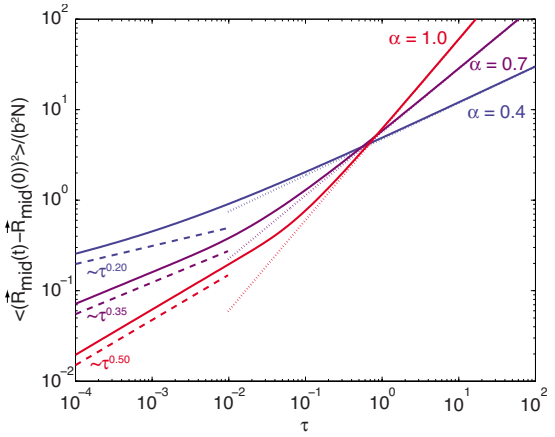

FIG. 2. (Color online) MSD for the midpoint monomer $\langle[\vec{R}_{\rm mid}(t)-\vec{R}_{\rm mid}(0)]^2\rangle/(b^2N)$ on an fLm polymer versus the dimensionless time $\tau=t/[N^2b^2\xi/(k_BT)]^{1/\alpha}$ for $\alpha=1.0$ (red), $\alpha=0.7$ (purple), and $\alpha=0.4$ (blue). Solid curves are solutions to the analytical result in Eq. (24) for these three α values. The dotted curves correspond to the long-time asymptotic behavior and the dashed curves give the short-time scaling of $\tau^{\alpha/2}$.

$$E_{\alpha,\beta}(x)=\sum_{j=0}^{\infty}\frac{x^j}{\Gamma(\beta+\alpha j)} \tag{22}$$

and $\beta=1$ in Eq. (21). The generalized Mittag-Leffler function for $\beta=1$ gives the regular Mittag-Leffler function (or just the Mittag-Leffler function); however, we define the generalized Mittag-Leffler function for use later in this paper. In the limit $\alpha\to1$, the correlation function is $C_p(t)=(3k_BT/k_p)\exp[-k_pt/(N\xi)]$, which corresponds to the behavior of the Rouse model in a Newtonian fluid [1]. However, in a viscoelastic fluid, where $0<\alpha<1$, the correlation function decays more slowly than an exponential, characteristically as a stretched exponential at short times and as an inverse power law at long times [21].

The $p=0$ solution is found by noting that $\vec{X}_0$ is the polymer center-of-mass. Since the polymer is free draining (no hydrodynamic interactions), the center-of-mass motion is that of an effective particle with total drag coefficient $N\xi$. Thus, the MSD is given by

$$\langle[\vec{X}_0(t)-\vec{X}_0(0)]^2\rangle=\frac{3k_BT}{N\xi}\frac{\sin(\alpha\pi)}{\pi\left(1-\frac{\alpha}{2}\right)(1-\alpha)\alpha}t^\alpha. \tag{23}$$

Our analysis facilitates the determination of the MSD of an individual monomer in the chain, which corresponds to the experimentally realizable case of tracking an individual locus on the *E. coli* chromosome. We define the midpoint monomer $\vec{R}_{\rm mid}(t)=\vec{r}(N/2,t)$, which behaves like all other monomers except the end points, $0\le n\le N$. Using our results, we find the MSD to be given by

$$\begin{aligned}\langle[\vec{R}_{\rm mid}(t)-\vec{R}_{\rm mid}(0)]^2\rangle&=\langle[\vec{X}_0(t)-\vec{X}_0(0)]^2\rangle+2\sum_{p=1}^{\infty}\langle[\vec{X}_{2p}(t)-\vec{X}_{2p}(0)]^2\rangle\\&=\frac{3k_BT}{N\xi}\frac{\sin(\alpha\pi)}{\pi\left(1-\frac{\alpha}{2}\right)(1-\alpha)\alpha}t^\alpha\\&\quad+\sum_{p=1}^{\infty}\frac{12k_BT}{k_{2p}}\left\{1-E_{\alpha,1}\left[-\frac{k_{2p}}{N\xi\Gamma(3-\alpha)}t^\alpha\right]\right\},\end{aligned} \tag{24}$$

where $k_{2p}=[3\pi^2k_BT/(Nb^2)](2p)^2$.

Figure 2 plots $\langle[\vec{R}_{\rm mid}(t)-\vec{R}_{\rm mid}(0)]^2\rangle/(b^2N)$ against the dimensionless time $\tau=t/[N^2b^2\xi/(k_BT)]^{1/\alpha}$ for three values of the scaling parameter α. Noting that $E_{\alpha,1}(-x)\to0$ as $x\to\infty$, the long-time limiting behavior of Eq. (24) is

$$\langle[\vec{R}_{\rm mid}(t)-\vec{R}_{\rm mid}(0)]^2\rangle\to\frac{3k_BT}{N\xi}\frac{\sin(\alpha\pi)}{\pi\left(1-\frac{\alpha}{2}\right)(1-\alpha)\alpha}t^\alpha. \tag{25}$$

This limiting behavior is shown in Fig. 2 as the dotted curves for each α-value. The short-time scaling $\langle[\vec{R}_{\rm mid}(t)-\vec{R}_{\rm mid}(0)]^2\rangle/(b^2N)\sim\tau^{\alpha/2}$ is identified in Fig. 2 by the dashed curves.

The physical justification for the short-time and long-time behaviors is determined by a scaling analysis of Eq. (24). The pth normal mode corresponds to a wavelength $\lambda=bN/p$. Each term within the summation in Eq. (24) represents the contribution of each normal mode to the displacement. The argument of the Mittag-Leffler function (i.e., $E_{\alpha,1}$) within the pth term identifies whether the $2p$th mode remains correlated at time t. Thus, we can identify a time scale t_λ for the relaxation of a wavelength λ by setting the argument to be order unity. This gives

$$t_\lambda\sim\left(\frac{\lambda^2\xi}{k_BT}\right)^{1/\alpha}\quad\text{or}\quad\lambda\sim\left(\frac{k_BT}{\xi}\right)^{1/2}t_\lambda^{\alpha/2}, \tag{26}$$

which neglects numerical factors from this scaling argument. At the time scale t_λ, sections of chain at lengths shorter than λ move in a coordinated fashion, since the corresponding short wave modes can respond to deformation at these times. Thus, a monomer feels an effective drag coefficient $\xi_\lambda\sim\xi\lambda/b$ at time t_λ. The resulting MSD at time t_λ scales as

$$\langle[\vec{R}_{\rm mid}(t_\lambda)-\vec{R}_{\rm mid}(0)]^2\rangle\sim\frac{k_BT}{\xi_\lambda}t_\lambda^\alpha\sim b\left(\frac{k_BT}{\xi}\right)^{1/2}t_\lambda^{\alpha/2}, \tag{27}$$

or in dimensionless form, we write

$$\langle[\vec{R}_{\rm mid}(t)-\vec{R}_{\rm mid}(0)]^2\rangle/(b^2N)\sim\tau^{\alpha/2}. \tag{28}$$

This regime persists until $\lambda\to bN$, defining the terminal time scale $t_R=[N^2b^2\xi/(k_BT)]^{1/\alpha}$. The dimensionless time is therefore identified as $\tau=t/t_R$, and the short-time scaling is valid for $\tau\ll1$. This limiting form is demonstrated in Fig. 2.

At times $\tau \gg 1$, the entire chain moves in a coordinated fashion, and the monomer displacement scales identically to the displacement of the polymer center-of-mass. Since our model neglects long-range hydrodynamic interactions (i.e., free-draining behavior), the total drag on the chain is $\xi_{tot} = N\xi$. The long-time limit of Eq. (24), given by Eq. (25), is exactly that of a single particle [Eq. (10)] with an effective drag coefficient ξ_{tot}.

We now proceed in our analysis to more directly address the impact of memory on the monomer trajectory. Toward this end, we define the velocity autocorrelation function $C_v(t) = \langle \vec{V}(t) \cdot \vec{V}(0) \rangle$, which gives a direct indicator of how previous motion impacts current motion. Thus, it can be calculated from experimental data and used as a diagnostic for fLm. We first consider C_v for a single particle, which is governed by the single-particle equation of motion [Eq. (7)]. The Laplace transform of Eq. (7) from t to s gives

$$\tilde{\vec{V}}(s) = \frac{1}{\xi \Gamma(3-\alpha)} s^{1-\alpha} \tilde{\vec{F}}^{(B)}(s), \tag{29}$$

where the tilde is used to indicate Laplace transform of the function, and $\vec{V}(t) = \frac{d\vec{R}(t)}{dt}$ is the particle velocity. This is used to find the average quantity

$$\langle \tilde{\vec{V}}(s) \cdot \tilde{\vec{V}}(s') \rangle = \frac{1}{[\xi \Gamma(3-\alpha)]^2} s^{1-\alpha} s'^{1-\alpha} \langle \tilde{\vec{F}}^{(B)}(s) \cdot \tilde{\vec{F}}^{(B)}(s') \rangle. \tag{30}$$

Using the fluctuation-dissipation theorem [Eq. (9)], we find

$$\langle \tilde{\vec{V}}(s) \cdot \tilde{\vec{V}}(s') \rangle = \frac{3k_B T}{\xi \Gamma(3-\alpha)} \frac{s s'^{2-\alpha} + s^{2-\alpha} s'}{s s' (s+s')}. \tag{31}$$

Upon Laplace inversion, we arrive at the solution

$$C_v(t) = -\frac{3k_B T}{\xi} \frac{\sin(\alpha\pi)}{\pi(2-\alpha)} |t|^{\alpha-2}. \tag{32}$$

The negative value of C_v arises from the viscoelastic response captured within the memory kernel. Particle motion incurs an elastic component to the response, leading to subsequent motion being pushed back toward the point of origin, thus a negative-valued C_v. This memory decays in time, as does $C_v(t)$.

The value of $C_v(t)$ diverges in the limit of $t \to 0$. This arises due to the fact that the instantaneous velocity is an ill-defined quantity for a Brownian random walk as defined by the overdamped Langevin equation [Eq. (7)]. Ultimately, inertial effects are not negligible at sufficiently small times, and the result must be consistent with that found from the Maxwell-Boltzmann distribution $C_v(0) = \frac{3k_B T}{m}$, where m is the particle mass. The behavior at $t=0$ cannot be resolved in our inertia-less treatment; however, the $t \neq 0$ behavior is correctly captured provided inertial effects are sufficiently damped at the time of interest.

Experimental measurement of C_v generally requires an approximation to the instantaneous velocity because particle position is measured at discrete time intervals (δ). To facilitate accurate comparison to experiments, we find the average quantity

$$C_v^{(\delta)}(t) = \frac{1}{\delta^2} \langle [\vec{R}(t+\delta) - \vec{R}(t)] \cdot [\vec{R}(\delta) - \vec{R}(0)] \rangle$$
$$= \begin{cases} \dfrac{C_v(t)}{\eta^2 \alpha(1-\alpha)} [2 - (1-\eta)^\alpha - (1+\eta)^\alpha], & t \geq \delta \\ \dfrac{C_v(t)}{\eta^2 \alpha(1-\alpha)} [2 + (\eta-1)^\alpha - (\eta+1)^\alpha] & \\ + \dfrac{3k_B T}{\xi} \dfrac{\sin(\alpha\pi)}{\pi\left(1-\frac{\alpha}{2}\right)(1-\alpha)\alpha} \dfrac{1}{\delta^2} (\delta - t)^\alpha, & t < \delta \end{cases} \tag{33}$$

where $\eta = \delta/t$. This quantity approaches $C_v(t)$ in the limit $\delta \to 0$ for $t \geq \delta$. The behavior for $t < \delta$ is valid for sufficiently large values of δ, such that inertial effects remain negligible for times $t < \delta$.

We now turn to the velocity autocorrelation function for the midpoint monomer of the fLm polymer $C_v^{(\mathrm{mid})}(t) = \langle \vec{V}_{\mathrm{mid}}(t) \cdot \vec{V}_{\mathrm{mid}}(0) \rangle$. To determine this correlation function, we define the mode velocity $\vec{V}_p(t) = \frac{d\vec{X}_p(t)}{dt}$. In finding $C_v^{(\mathrm{mid})}$, we find $\langle \vec{V}_p(t) \cdot \vec{V}_p(0) \rangle$ directly from our results for $C_p(t)$ found in Eq. (21). With this and similar steps as used to find C_v, we arrive at

$$C_v^{(\mathrm{mid})}(t) = \langle \vec{V}_0(t) \cdot \vec{V}_0(0) \rangle + 2 \sum_{p=1}^{\infty} \langle \vec{V}_{2p}(t) \cdot \vec{V}_{2p}(0) \rangle$$
$$= -\frac{3k_B T}{N\xi} \frac{\sin(\alpha\pi)}{\pi(2-\alpha)} |t|^{\alpha-2} \times \left\{ 1 + 2\gamma(\alpha-1) \sum_{p=1}^{\infty} E_{\alpha,\alpha-1}\left[-\frac{k_{2p}}{N\xi\Gamma(3-\alpha)} t^\alpha \right] \right\}. \tag{34}$$

Noting that $E_{\alpha,\alpha-1}(-x) \to 0$ as $x \to \infty$, we find the long-time asymptotic behavior of Eq. (34) to be

$$C_v^{(\mathrm{mid})}(t) \to -\frac{3k_B T}{N\xi} \frac{\sin(\alpha\pi)}{\pi(2-\alpha)} |t|^{\alpha-2} \tag{35}$$

for $t \gg t_R$. The short-time scaling of Eq. (34), which will be discussed below, is given by

$$C_v^{(\mathrm{mid})}(t)/(Nb^2/t_R^2) \sim \tau^{(\alpha/2)-2} \tag{36}$$

for $t \ll t_R$.

As in the MSD, we use scaling analyses to understand the short-time and long-time behaviors. Equation (34) features a summation over p modes, representing the contribution of the Rouse modes within the polymer. The argument of the Mittag-Leffler function $E_{\alpha,\alpha-1}$ identifies the time scale t_λ for relaxation of a Rouse mode of wavelength $\lambda = bN/p$. As previously discussed, monomers within the wavelength λ respond dynamically at the time scale t_λ, thus they move coherently. As a result, a monomer feels an effective drag coefficient $\xi_\lambda \sim \xi\lambda/b \sim (\xi k_B T)^{1/2} t_\lambda^{\alpha/2}/b$ at time t_λ. Using the result for C_v for a particle [Eq. (32)], the scaling of $C_v^{(\mathrm{mid})}$ at time t_λ scales as

$$C_v^{(\mathrm{mid})}(t_\lambda) \sim -\frac{k_B T}{\xi_\lambda} t_\lambda^{\alpha-2} \sim -b\left(\frac{k_B T}{\xi}\right)^{1/2} t_\lambda^{\tau^{(\alpha/2)-2}}. \quad (37)$$

In dimensionless form, we have $C_v(t)/(Nb^2/t_R^2) \sim \tau^{\tau^{(\alpha/2)-2}}$ (i.e., Eq. (36)), where $\tau = t/t_R$, and $t_R = [N^2 b^2 \xi/(k_B T)]^{1/\alpha}$ is the terminal relaxation time, where all Rouse modes are relaxed and the entire chain moves coherently. This short-time scaling is valid for $\tau \ll 1$.

For times $\tau \gg 1$, the monomer motion is coherent with the motion of the entire chain. Thus, $C_v^{(\mathrm{mid})}$ tends toward that of a particle with effective drag $\xi_{tot} = N\xi$. This behavior leads directly to the long-time asymptotic form of $C_v^{(\mathrm{mid})}(t)$ given by Eq. (35).

This section provides the fundamental framework for analyzing the Rouse modes of a fLm polymer. Theoretical predictions for the monomer MSD scaling and the velocity autocorrelation function provide diagnostic tools that can be compared with experimental measurements to determine whether fLm is the dominant physical mechanism for subdiffusion. We show that a negative value of the velocity autocorrelation function is prevalent for both a particle and a polymer undergoing fLm.

V. POLYMER SUBJECT TO RANDOM WAITING

In this section, we address random waiting in a polymer as an alternative model for subdiffusive motion. In a continuous time random walk (CTRW) [22], a diffusing particle experiences random pause events where it waits a time t before re-engaging in its motion. If the waiting-time distribution has long tails, such that the ensemble-average waiting time $\langle t \rangle_{\mathrm{wait}}$ diverges, then the overall motion becomes subdiffusive. Though this model is consistent with some aspects of particle motion in a cell [14], it remains to be established whether a polymer that is composed of monomers that undergo transient waiting is a suitable model for the anomalous motion of a monomer within a polymer. Our goal in this section is to develop the framework for analyzing the motion of a polymer that is subject to random waiting (i.e., CTRW) in order to interpret the feasibility of this model.

We first consider a single, isolated particle that undergoes Brownian motion in a Newtonian fluid while vascillating between *diffusing* and *waiting* states. Our adopted model for the distribution of time spent in the *diffusing* state is governed by

$$S_{\mathrm{diff}}(t)dt = \frac{1}{t_{\mathrm{diff}}} \exp\left(-\frac{t}{t_{\mathrm{diff}}}\right) dt, \quad (38)$$

which gives the probability that if the particle transitions from the *waiting* state to the *diffusing* state at time zero that it will transition from the *diffusing* state to the *waiting* state between time t and $t+dt$. The parameter t_{diff} is equal to the ensemble-average time spent in the *diffusing* state [i.e., $\langle t \rangle_{\mathrm{diff}} = t_{\mathrm{diff}}$, where the subscript *diff* is an average w.r.t. Eq. (38)]. In this section, the angle brackets $\langle \ldots \rangle$ imply an ensemble average, which is frequently not equal to the time average.

The analogous distribution that we adopt for the *waiting* state is

$$S_{\mathrm{wait}}(t)dt = \begin{cases} \dfrac{\alpha}{\alpha+1}\dfrac{1}{t_{\mathrm{wait}}} dt, & t < t_{\mathrm{wait}} \\ \dfrac{\alpha}{\alpha+1}\dfrac{1}{t_{\mathrm{wait}}}\left(\dfrac{t_{\mathrm{wait}}}{t}\right)^{\alpha+1} dt, & t \geq t_{\mathrm{wait}}, \end{cases} \quad (39)$$

where the power-law tail in the transition time is governed by the scaling constant α. For $\alpha > 1$, the parameter t_{wait} results in the ensemble-average time spent in the *waiting* state $\langle t \rangle_{\mathrm{wait}} = t_{\mathrm{wait}}\alpha/[2(\alpha-1)]$, where the subscript *wait* is an average w.r.t. Eq. (39). For $0 < \alpha \leq 1$, the ensemble-average time spent in the *waiting* state is infinity; therefore, $\alpha = 1$ is a critical point in the behavior of this model.

The motion of the particle position $\vec{R}(t)$ is governed by the equation of motion

$$\xi \frac{d\vec{R}(t)}{dt} = \sigma^{(\mathrm{diff})}(t)\vec{F}^{(B)}(t), \quad (40)$$

where $\sigma^{(\mathrm{diff})}(t) = 1$ if the particle is in the *diffusing* state at time t, and $\sigma^{(\mathrm{diff})}(t) = 0$ if the particle is in the *waiting* state at time t. The times spent in the *diffusing* and *waiting* states are selected from $S_{\mathrm{diff}}(t)$ and $S_{\mathrm{wait}}(t)$, respectively. The Brownian force $\vec{F}^{(B)}(t)$ satisfies the fluctuation-dissipation theorem for diffusion in a Newtonian fluid

$$\langle \vec{F}^{(B)}(t)\vec{F}^{(B)}(t') \rangle = 2\xi k_B T \delta(t-t')\mathbf{I}. \quad (41)$$

The particle motion is analyzed using methods that we develop for the behavior of a two-state reaction-diffusion model; we refer the reader to Ref. [23] for details. Using these methods, the Brownian motion of our model gives a MSD of the particle

$$\langle [\vec{R}(t) - \vec{R}(0)]^2 \rangle = \begin{cases} \dfrac{6k_B T}{\xi} \dfrac{1}{1 + \dfrac{\alpha}{2(\alpha-1)}\dfrac{t_{\mathrm{wait}}}{t_{\mathrm{diff}}}} t, & \alpha > 1 \\ \dfrac{6k_B T t_{\mathrm{diff}}}{\xi} \dfrac{(1+\alpha)\sin(\alpha\pi)}{\alpha\pi} \left(\dfrac{t}{t_{\mathrm{wait}}}\right)^{\alpha}, & 0 < \alpha < 1. \end{cases} \quad (42)$$

We note that this functional form approaches zero for $\alpha \to 1$ from both the negative ($\alpha \to 1^-$) and positive ($\alpha \to 1^+$) directions. This notable idiosyncrasy is reconciled by the fact that the time required to achieve this limiting behavior also diverges for $\alpha \to 1$. The overall observation is that the particle behaves diffusively for $\alpha \geq 1$ and subdiffusively for $0 < \alpha < 1$ with a MSD that scales as t^α.

The behavior for $\alpha > 1$ is justified by noting that the ensemble-averaged probability of being in the *diffusing* state for $\alpha > 1$ is $\langle \sigma^{(\mathrm{diff})}(t \to \infty) \rangle = t_{\mathrm{diff}}/\{t_{\mathrm{diff}} + t_{\mathrm{wait}}\alpha/[2(\alpha-1)]\}$. Thus, the $\alpha > 1$ behavior is exactly the free diffusion behavior $(6k_B T/\xi)t$ times the fraction of time spent in the *diffusing* state.

The subdiffusive behavior that arises for $0 < \alpha < 1$ occurs due to the ergodicity breaking that arises from the *waiting*-time distribution. For large time, the ensemble-averaged

probability of being in the *diffusing* state for $0<\alpha<1$ approaches

$$\langle \sigma^{(\mathrm{diff})}(t)\rangle \to \frac{(1+\alpha)\sin(\alpha\pi)}{\pi}\frac{t_{\mathrm{diff}}}{t_{\mathrm{wait}}^{\alpha}}\frac{1}{t^{1-\alpha}}. \tag{43}$$

The power-law tail in S_{wait} leads to the ensemble-averaged *diffusing*-state probability approaching zero at large time, thus indicating an inequality between the ensemble average and time average indicative of an ergodicity breaking. This nonergodic behavior has significant consequences for the material exchange between a reactive surface and the bulk, as may be the case for a DNA-binding protein [24,25]. While a particle is in the *diffusing* state, the time rate-of-change of the MSD is $d[\langle[\vec{R}(t)-\vec{R}(0)]^2\rangle]/dt=(6k_BT/\xi)$, which is the result for a freely diffusing particle without waiting. The time rate-of-change of the MSD for the CTRW particle with $0<\alpha<1$ is given by the *diffusing*-state rate-of-change in the previous sentence times the probability of being in the *diffusing* state; thus,

$$\frac{d\langle[\vec{R}(t)-\vec{R}(0)]^2\rangle}{dt} = \frac{6k_BT}{\xi}\langle\sigma^{(\mathrm{diff})}(t)\rangle = \frac{6k_BT}{\xi}\frac{(1+\alpha)\sin(\alpha\pi)}{\pi}\frac{t_{\mathrm{diff}}}{t_{\mathrm{wait}}^{\alpha}}\frac{1}{t^{1-\alpha}}, \tag{44}$$

which is in exact agreement with Eq. (42) for $0<\alpha<1$.

We now consider the motion of a large linear polymer that is subject to random waiting, moving as a CTRW. In this treatment, we address the Rouse modes within a CTRW polymer, neglecting self-interaction and hydrodynamic interaction. The equation of motion is given by

$$g\xi\frac{d\vec{R}_m(t)}{dt} = \sigma_m^{(\mathrm{diff})}(t)[\vec{F}_m^{(E)}(t)+\vec{F}_m^{(B)}(t)], \tag{45}$$

where $\sigma_m^{(\mathrm{diff})}(t)=1$ if the mth monomer in the chain is in the *diffusing* state at time t, and $\sigma_m^{(\mathrm{diff})}(t)=0$ if the mth monomer is in the *waiting* state at time t $(m=0,1,2,\ldots,M)$. In this model, there are two contributions to subdiffusive motion. The first contribution is the ergodicity breaking inherent in the CTRW model when $0<\alpha<1$, and the second contribution is associated with the relaxation of the internal Rouse modes of the polymer.

Equation (45) permits the evaluation of trajectories of a CTRW polymer in time. Our approach to solving this equation of motion is to perform a numerical time integration of the equation of motion (as in a Brownian dynamics simulation), determining the transitions between diffusing and waiting states based on the governing statistical distributions [Eqs. (38) and (39)]. We verify this algorithm by comparison with our exact results for particle diffusion [Eq. (42)] by performing a series of particle simulations ($M=1$, data not shown).

In the case $0<\alpha<1$, each individual monomer within the polymer chain exhibits ergodicity breaking with a long-time probability of being in the *diffusing* state given by Eq. (43). The polymer is capable of moving via two distinct mechanisms. If all of the monomers are in the *diffusing* state, the polymer moves according to a *free-diffusion* mechanism, where the motion is diffusive with an effective drag coefficient $g(M+1)\xi$. If at least one monomer is in the *waiting* state, the polymer must move according to a *pin-and-pivot* mechanism, where the unfrozen segments crawl while frozen segments pin parts of the polymer in space. These two mechanisms contribute to the mid-point monomer MSD, which we define as $\mathrm{MSD}_{\mathrm{mid}}=\langle[\vec{R}_{\mathrm{mid}}(t)-\vec{R}_{\mathrm{mid}}(0)]^2\rangle$.

The probability that all monomers are in the *diffusing* state is $\langle\sigma^{(\mathrm{diff})}(t)\rangle^{M+1}$, which tends to zero as $1/t^{(M+1)(1-\alpha)}$. The *free-diffusion* mechanism results in a time rate-of-change for the midpoint-monomer MSD that scales as

$$\frac{d\langle[\vec{R}_{\mathrm{mid}}(t)-\vec{R}_{\mathrm{mid}}(0)]^2\rangle}{dt} \sim \frac{k_BT}{g(M+1)\xi}\langle\sigma^{(\mathrm{diff})}(t)\rangle^{M+1} \sim \frac{k_BT}{g(M+1)\xi}\frac{t_{\mathrm{diff}}^{M+1}}{t_{\mathrm{wait}}^{(M+1)\alpha}}\frac{1}{t^{(M+1)(1-\alpha)}}. \tag{46}$$

From this analysis, we find the long-time scaling behavior of $\mathrm{MSD}_{\mathrm{mid}}$ to be

$$\langle[\vec{R}_{\mathrm{mid}}(t)-\vec{R}_{\mathrm{mid}}(0)]^2\rangle \sim \frac{k_BT}{g(M+1)\xi}\frac{t_{\mathrm{diff}}^{M+1}}{t_{\mathrm{wait}}^{(M+1)\alpha}}t^{\alpha_{\mathrm{FD}}}, \tag{47}$$

where α_{FD} is the *free-diffusion* scaling parameter

$$\alpha_{\mathrm{FD}} = \begin{cases} 1-(M+1)(1-\alpha), & M<M_c \\ 0, & M\geq M_c \end{cases} \tag{48}$$

with $M_c=1+1/(1-\alpha)$ being the critical monomer number. This result suggests that the scaling behavior depends on the number of monomers (or length of chain). Furthermore, for any appreciable length of chain ($M\geq M_c$), this is not a viable transport mechanism, since ergodicity breaking leads to a cessation in the motion.

The *pin-and-pivot* mechanism permits motion to occur under conditions where multiple monomers are frozen in the *waiting* state. The net scaling of the MSD for this mechanism is not easily reconciled through a scaling analysis due to the complexity associated with the ergodicity breaking and the coordinated dynamics. For this paper, we demonstrate these mechanisms through numerical simulations. In Fig. 3, we show the results for the midpoint-monomer MSD from an ensemble average over 1000 simulations for several lengths of chain. Parameters for these simulations are $k_BT=1$, $g=1$, $b=0.5477$, $\xi=1$, $t_{\mathrm{diff}}=1$, $t_{\mathrm{wait}}=1$, and $\alpha=0.7$, and we perform experiments for 1 monomer ($M=0$), 2 monomers ($M=1$), 3 monomers ($M=2$), 4 monomers ($M=3$), and 100 monomers ($M=99$). Included in Fig. 3 are our predictions for the *free-diffusion* mechanisms, governed by the scaling parameter α_{FD} for 1 monomer ($\alpha_{\mathrm{FD}}=0.7$), 2 monomers ($\alpha_{\mathrm{FD}}=0.4$), and 3 monomers ($\alpha_{\mathrm{FD}}=0.1$). The short-time behavior is diffusive (i.e., $\mathrm{MSD}_{\mathrm{mid}}\sim t$) for all simulations due to the discrete nature of the model setting a short-time cutoff for the Rouse modes.

The results shown in Fig. 3 demonstrate the chain-length dependence of the scaling behavior of $\mathrm{MSD}_{\mathrm{mid}}$. Our simple analysis of the *free-diffusion* mechanism is accurate for chains with 2 monomers. However, we predict the dominant

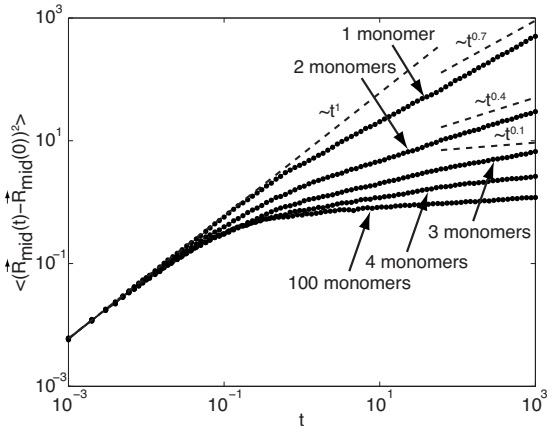

FIG. 3. Ensemble-averaged MSD of the midpoint monomer on a CTRW polymer versus time t. Data are from a series of simulations with an increasing number of monomers: $M=0$, $M=1$, $M=2$, $M=3$, and $M=99$ (see text for parameter values). Dotted lines correspond to the *free-diffusion* scaling $\mathrm{MSD}_{\mathrm{mid}} \sim t^{\alpha_{\mathrm{FD}}}$; deviations from this prediction are indicative of the *pin-and-pivot* mechanism. The dashed line gives the short-time scaling of $\mathrm{MSD}_{\mathrm{mid}} \sim t^1$ that is common to all simulations.

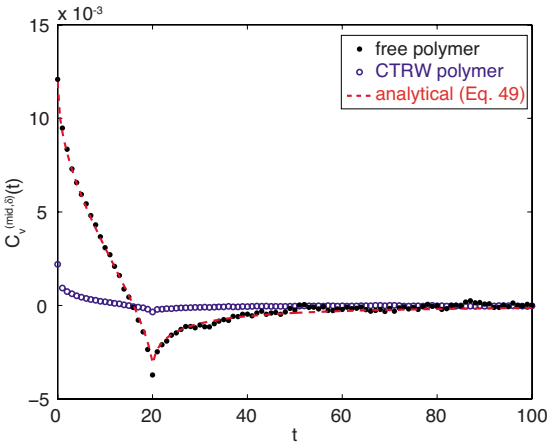

FIG. 4. (Color online) Velocity autocorrelation function of the midpoint monomer $C_v^{(\mathrm{mid},\delta)}$ versus time t. Data are from simulations of a free polymer chain (black filled circels) and a CTRW polymer (blue open circles), where $\delta=20$. The red dashed curve corresponds to the analytical result in Eq. (49) for a free polymer chain, with the dip at $t=20$ indicative of the Rouse elasticity.

mechanism of motion for chains with more than 3 monomers is the *pin-and-pivot* mechanism. These results assume that monomer waiting is entirely uncorrelated and force independent. While these assumptions may not hold at short length scales, many experiments of interest involve polymers that are sufficiently large such that uncorrelated waiting times would occur for many segments of the chain. Our results in Fig. 3 demonstrate that a chromosome with only four segments that wait independently moves by the *pin-and-pivot* mechanism with similar behavior for its MSD as if it had 100 independent waiting segments. Therefore, our results have a wide range of applicability in chromosome-length phenomena. It may also be interesting to explore the effect of correlated waiting times, as recently addressed for particle motion [26].

In the previous section, we identify the velocity autocorrelation function C_v as a suitable metric to determine the impact of memory on the monomer motion. There is no inherent memory for a CTRW particle whose motion is governed by Eq. (40); thus, the resulting velocity autocorrelation function $C_v(t)$ is zero for all $t \neq 0$.

In the case of the CTRW polymer, the elasticity of the polymer results in Rouse relaxation modes, contributing memory to the motion. However, it is unclear how random waiting will impact the memory (or C_v). As a comparison, we note that the midpoint-monomer velocity autocorrelation function for polymer in the absence of random waiting is given by

$$C_v^{(\mathrm{mid})} = -\frac{6k_BT}{N^2\xi^2}\sum_{p=1}^{\infty} k_{2p} \exp\left(-\frac{k_{2p}}{N\xi}t\right), \tag{49}$$

where $k_{2p}=[3\pi^2 k_B T/(Nb^2)](2p)^2$. This behavior is found by taking the limit of Eq. (34) as $\alpha \to 1$. We adapt this to the approximate form $C_v^{(\mathrm{mid},\delta)} = \frac{1}{\delta^2}\langle[\vec{R}_{\mathrm{mid}}(t+\delta)-\vec{R}_{\mathrm{mid}}(t)]\cdot[\vec{R}_{\mathrm{mid}}(\delta) - \vec{R}_{\mathrm{mid}}(0)]\rangle$ using similar steps as used to find Eq. (33).

In Fig. 4, we show ensemble-average determination of the approximate velocity autocorrelation function $C_v^{(\mathrm{mid},\delta)}$ (with $\delta=20$) from simulations of a free polymer chain (i.e., no random waiting) and a CTRW polymer. In both simulations, we use $k_BT=1$, $\xi=1$, $b=0.5477$, $g=1$, and $M=99$, and the CTRW polymer is subjected to random waiting with $t_{\mathrm{diff}}=1$ and $t_{\mathrm{wait}}=1$. Figure 4 clearly demonstrates that the introduction of random waiting into the polymer dramatically suppresses the elastic memory within the polymer chain. The free polymer exhibits a large negative $C_v^{(\mathrm{mid},\delta)}$; whereas, the CTRW polymer has a peak negative value at $t=20$ that is less than one tenth that of the free polymer. We find similar results for a CTRW polymer under confinement, with $C_v^{(\mathrm{mid},\delta)}(t=20)$ only 1.5-fold more negative than the unconfined CTRW polymer and still approximately tenfold smaller than the free polymer.

The physical justification for the suppression of $C_v^{(\mathrm{mid},\delta)}$ for the CTRW polymer lies in the impact of waiting on the internal relaxation times. The free polymer undergoes Rouse-mode relaxation with longer wavelengths requiring longer time to relax. However, the waiting associated with the CTRW polymer eliminates the long wave modes from the relaxation dynamics by pinning sections of the chain in space. The distance between pinned monomers dictates the local relaxation dynamics rather than the natural Rouse mode at any given time scale. Since this pinned length scale is always much less than the chain length, particularly under conditions of ergodicity breaking ($0<\alpha<1$), this relaxation time is effectively instantaneous, and the memory effects within the polymer are almost entirely suppressed.

As the velocity autocorrelation function is easily measured experimentally, we propose that the behavior of this property could be generally used as a diagnostic to distinguish underlying CTRW versus fLm mechanisms leading to subdiffusion of biological polymers in living cells.

VI. CONCLUSIONS

This manuscript explores the consequences of confinement, viscoelasticity, and binding interactions on the motion of monomers in a polymer. These three physical contributions are relevant to the behavior of a wide range of biological macromolecules, including the bacterial chromosome. Our goal is to incorporate these physical effects into the classical description of polymer dynamics to better understand their role in biological phenomena.

In Sec. III, we use numerical simulations to investigate how confinement and self-interaction affect the motion of monomers on a single polymer. The Rouse, Zimm, and reptation models address various aspects of polymer motion under dilute, semi-dilute, and concentrated conditions; it is not immediately obvious what role these dynamic models play in our current problem. Our simulation results suggest the Rouse model adequately captures the monomer MSD for intermediate time scales, up to the terminal time where the monomer MSD reaches the confinement length scale. Although reptation seems to be a likely model for the self-slithering motion of a single polymer chain, we conclude that the correlated motion of the confined chain annihilates its own reptation tube, eliminating this dynamic mechanism. Therefore, the monomer MSD for a single confined polymer in a Newtonian fluid is expected to scale as $t^{0.5}$ for intermediate time scales.

In Sec. IV, we study the role of environment viscoelasticity on the dynamics of a single polymer by introducing a fLm memory function into the monomer drag force. Given the dominant role that the Rouse model plays in the confined polymer, we focus our analysis on the Rouse modes of a fLm polymer. The model introduces the parameter α as the MSD scaling for an individual fLm particle (i.e., MSD$\sim t^{\alpha}$). A polymer chain that is composed of such fLm monomers exhibits a monomer MSD with a short-time scaling of $\frac{\alpha}{2}$ (for times up to the longest relaxation time $t_R=[N^2b^2\xi/(k_BT)]^{1/\alpha}$).

As a further test of our predictions, we introduce the velocity autocorrelation function C_v as a metric for the environmental memory. A hallmark feature of memory in a viscoelastic fluid is a negative-valued C_v at intermediate time scales. Our results in Sec. IV conclude that a fLm particle exhibits the scaling $C_v\sim -t^{\alpha-2}$ and the midpoint monomer in a fLm polymer has the scaling $C_v\sim -t^{(\alpha/2)-2}$.

Our final analysis in Sec. V addresses the role of transient waiting in the motion of a monomer in the polymer chain. We draw two primary conclusions for a polymer subjected to random waiting (CTRW polymer). The first conclusion is that a polymer chain that experiences random waiting exhibits considerable arrest in the motion of an individual monomer. Waiting in a long polymer chain hinders motion due to a need to coordinate motion between multiple monomers for a monomer to move. Ergodicity breaking leads to the probability of coordinated motion approaching zero at long times, thus dramatically suppressing the monomer motion. The second conclusion is that random waiting within a polymer chain suppresses the memory effects associated with the elastic relaxation processes of the polymer chain. This is due to the arrest of long wave mode relaxations when multiple points on the chain are pinned.

Our results in this paper conclude that subdiffusive monomer motion leads to widely varying behavior for a polymer depending on the root cause of the monomer subdiffusion. Particle motion leads to ensemble-averaged MSD that is the same for fLm and CTRW models, and one needs to turn to other average properties to determine whether an ensemble of trajectories are governed by fLm or CTRW models [12,14–16]. However, these models are easily distinguishable for a polymer composed of subdiffusive monomers. The connectivity of a polymer results in new dynamic mechanisms that are dramatically influenced by the nature of the monomer motion, leading to different scaling behaviors for monomer MSD and C_v.

Our results can be compared directly to experimental observations. By tracking fluorescently labeled chromosomal loci in live cells, we and others have found an MSD scaling of $\sim$0.32–0.40 [2–5]. These α values are less than expected from the Rouse-like behavior of a polymer under confinement, as demonstrated by our simulations in Sec. III. Therefore, additional physical effects must be responsible for the observed subdiffusion. Our theoretical predictions in Secs. IV and V allow us to identify fLm as the dominant physical mechanism underlying the anomalous motion of chromosomal loci in *E. coli* [3]. The MSD scaling of chromosomal loci is approximately one-half that of an RNA-protein particle, which scales as $\sim$0.70–0.77 [3,9], i.e., particle scaling of α leads to polymer scaling $\sim\frac{\alpha}{2}$, as predicted for a fLm polymer. Furthermore, the ensemble-average and time-average MSD for both chromosomal loci and RNA-protein particles exhibit the same scaling, consistent with an ergodic process like fLm. Finally, $C_v<0$ at short-time lags [3], indicating memory, which is characteristic of a fLm polymer [Eq. (34)] but suppressed in a CTRW polymer. Thus, by incorporating two relatively simple models into the Rouse framework, we can distinguish among the prominent mechanisms for anomalous diffusion, as well as resolve the scaling discrepancy between particles [9,10] and polymers [2–5].

The agreement between our theory and experimental measurements [3] suggests that the Rouse model modified by the viscoelastic environment is the dominant dynamic mechanism for chromosome reorganization within *E. coli*, at least on time scales of the experimental measurements. This observation is critical in guiding the development of theories of the dynamics within a complex cellular environment. In this case, classic polymer models, when properly modified, render results that can clearly distinguish between candidate molecular processes for chromosome reorganization. These results represent an important example where we can leverage existing physical understanding of polymer dynamics to render quantitative predictions of *in vivo* phenomena.

ACKNOWLEDGMENTS

S.C.W was supported by an R. L. Kirschstein NRSA; A.J.S. was supported by NSF-Career Award; J.A.T. was supported by HHMI. This project was also supported by Grant No. AI-67712 from the National Institute of Allergy and Infectious Diseases. Its contents are soley the responsibility of the authors and do not necesarily represet the official view of the NIAID.

[1] M. Doi and S. F. Edwards, *The Theory of Polymer Dynamics* (Oxford University Press, New York, 1986).
[2] A. Fiebig, K. Keren, and J. A. Theriot, Mol. Microbiol. **60**, 1164 (2006).
[3] S. C. Weber, A. J. Spakowitz, and J. A. Theriot, Phys. Rev. Lett. **104**, 238102 (2010).
[4] G. G. Cabal *et al.*, Nature (London) **441**, 770 (2006).
[5] I. Bronstein, Y. Israel, E. Kepten, S. Mai, Y. Shav-Tal, E. Barkai, and Y. Garini, Phys. Rev. Lett. **103**, 018102 (2009).
[6] J. P. Bouchaud and A. Georges, Phys. Rep. **195**, 127 (1990).
[7] F. Gittes, B. Schnurr, P. D. Olmsted, F. C. MacKintosh, and C. F. Schmidt, Phys. Rev. Lett. **79**, 3286 (1997).
[8] D. S. Banks and C. Fradin, Biophys. J. **89**, 2960 (2005).
[9] I. Golding and E. C. Cox, Phys. Rev. Lett. **96**, 098102 (2006).
[10] I. M. Tolic-Nørrelykke, E. L. Munteanu, G. Thon, and L. Oddershede, K. Berg-Sørensen, Phys. Rev. Lett. **93**, 078102 (2004).
[11] M. J. Saxton, Biophys. J. **66**, 394 (1994).
[12] W. H. Deng and E. Barkai, Phys. Rev. E **79**, 011112 (2009).
[13] M. J. Saxton, Biophys. J. **70**, 1250 (1996).
[14] Y. He, S. Burov, R. Metzler, and E. Barkai, Phys. Rev. Lett. **101**, 058101 (2008).
[15] S. Condamin *et al.*, Proc. Natl. Acad. Sci. U.S.A. **105**, 5675 (2008).
[16] R. Metzler *et al.*, Acta Phys. Pol. B **40**, 1315 (2009).
[17] P. E. Rouse, J. Chem. Phys. **21**, 1272 (1953).
[18] B. H. Zimm, J. Chem. Phys. **24**, 269 (1956).
[19] P. G. de Gennes, J. Chem. Phys. **55**, 572 (1971).
[20] S. C. Kou and X. S. Xie, Phys. Rev. Lett. **93**, 180603 (2004).
[21] M. H. Vainstein, I. V. L. Costa, R. Morgado, and F. A. Oliveira, EPL **73**, 726 (2006).
[22] E. W. Montroll and G. H. Weiss, J. Math. Phys. **6**, 167 (1965).
[23] M. Díaz de la Rosa, E. F. Koslover, P. J. Mulligan, and A. J. Spakowitz, Biophys. J. **98**, 2943 (2010).
[24] M. A. Lomholt, I. M. Zaid, and R. Metzler, Phys. Rev. Lett. **98**, 200603 (2007).
[25] I. Zaid, M. Lomholt, and R. Metzler, Biophys. J. **97**, 710 (2009).
[26] V. Tejedor and R. Metzler, J. Phys. A: Math. Theor. **43**, 082002 (2010)..